

A MODEL FOR CALCULATING RATES OF GENERAL CORROSION OF CARBON STEEL AND 13%Cr STAINLESS STEEL IN CO₂/H₂S ENVIRONMENTS

Andrzej Anderko and Robert D. Young
OLI Systems Inc.
108 American Road
Morris Plains, NJ 07950

ABSTRACT

A model has been developed for calculating the rates of general corrosion of carbon steel and 13%Cr steel in aqueous systems containing carbon dioxide, hydrogen sulfide and other components. The model combines a comprehensive thermodynamic speciation module with electrochemical computations based on the mixed-potential theory. The electrochemical calculations recognize the effects of various partial cathodic and anodic processes and incorporate a model for the active-passive transition and the effect of solution species on passivity. The model has been verified by comparing calculated corrosion rates with experimental data over substantial ranges of temperature, pressure and solution composition. In particular, the effects of salinity, hydrogen sulfide and acetic acid on CO₂ corrosion can be simulated. Very good agreement with experimental data has been obtained. The model has been implemented in a program that makes it possible to analyze the effects of various environmental variables on the rates of general corrosion.

KEY WORDS: Modeling, thermodynamics, electrochemical kinetics, carbon steel, 13%Cr steel, CO₂/H₂S corrosion

INTRODUCTION

Corrosion of metals by carbon dioxide with or without other corrosive agents such as hydrogen sulfide is of significant interest in the oil and gas industry. The corrosion phenomena depend on a multitude of factors including the characteristics of metals, temperature, composition of aqueous streams, partial pressures of CO₂ and H₂S, flow conditions, etc. In view of the large number of independent variables, it is worthwhile to develop computational models that could summarize the available body of experimental information and, at the same time, make it possible to predict the

corrosion behavior at conditions for which corrosion rates have not been experimentally investigated. For CO₂ corrosion of carbon steels, several models have been reported in the literature.¹⁻¹⁴ These models have the form of semi-empirical correlations, expert systems or are based on electrochemical theory. No models have been published for 13%Cr steels.

In previous studies,^{15,16} we developed a model for general corrosion of carbon steels that combines a comprehensive thermodynamic module for speciation calculations with an electrochemical module for simulating the rates of corrosion processes at the metal/aqueous solution interface. The thermodynamic module predicts the activities of solution species and phase equilibria in the bulk solution whereas the electrochemical module considers partial cathodic and anodic reactions that determine the magnitude of corrosion rates. This approach made it possible to include systems with corrosive agents other than CO₂, such as hydrogen sulfide or acetic acid. In separate studies, this model was applied to other systems including concentrated brines¹⁷ and industrial water systems with inorganic inhibitors.¹⁸

In this study, we extend the applicability of this model to 13%Cr stainless steels. Then, we validate the model against experimental data and compare the performance of the model for carbon steel and 13%Cr steels.

THERMODYNAMIC CALCULATIONS

The starting point for the analysis of corrosion is the computation of speciation in the investigated system. For this purpose, a realistic thermodynamic model of electrolyte systems is used. This model combines information about standard-state properties of all species that may exist in the system with a formulation for the excess Gibbs energy, which accounts for solution nonideality. The model has been described in detail by Zemaitis et al.¹⁹ and Rafal et al.²⁰ The main elements of the model have also been summarized in our previous studies of CO₂/H₂S corrosion.^{15,16}

The thermodynamic model provides answers to the following questions:

- (1) What are the individual chemical species that exist in the system?
- (2) What are the phase equilibria in the system, i.e., how do the components partition between the aqueous, vapor and, possibly, solid and nonaqueous liquid phases?
- (3) What are the activities of individual species?

The activities of individual species are further used for electrochemical calculations. Since the rates of electrochemical processes depend on the activities of species such as H⁺, OH⁻, CO_{2(aq)}, Cl⁻, HS⁻, etc., their values must be accurately known as functions of temperature, pressure and overall mixture composition. In addition to thermodynamic properties, the thermodynamic module returns diffusion coefficients of individual species and viscosity of the solution.

ELECTROCHEMICAL CALCULATIONS

The electrochemical model takes into account various reactions on the surface of the metal and evaluates the current density versus potential relationships for each significant reaction. Then, the

model combines the partial processes to compute corrosion rates in the framework of the mixed-potential theory.

Partial electrochemical reactions

In previous papers,^{15,16} expressions were developed for the computation of current density versus potential relationships for partial electrochemical reactions that are responsible for the corrosion of iron and carbon steel in the active state. The cathodic reactions that are considered for CO₂/H₂S systems include:

- (1) Reduction of protons
- (2) Reduction of water molecules
- (3) Reduction of carbonic acid, which is preceded by a homogeneous reaction of hydration of dissolved carbon dioxide
- (4) Reduction of hydrogen sulfide

The anodic reaction of active dissolution includes:

- (1) The general mechanism of dissolution, which is mediated by the adsorption of hydroxide ions
- (2) Additional contributions due to the adsorption of active species such as bisulfide ions

The model also includes the effects of the formation of FeCO₃ and FeS scales on the partial processes. Detailed expressions for the current density versus potential relationships for these processes were given in previous papers^{15,16} and, therefore, will not be repeated here.

For the 13%Cr steels, it has been assumed that the expressions for the partial electrochemical processes in the active state, which were originally developed for carbon steels,^{15,16} can be used in the same mathematical form, but with different numerical values of characteristic parameters. It should be noted here that the expressions for partial electrode processes on the surface of carbon steel were shown to be in agreement with various mechanistic studies of the dissolution of iron in acidic, CO₂ and H₂S-containing media (cf. Anderko and Young,^{15,17} Anderko¹⁶ and references cited therein). In the case of 13%Cr steels, there is a dearth of comparable mechanistic studies. In the absence of mechanistic information, the use of the same expressions for the active dissolution of both classes of metals can be justified on the basis of the agreement of the obtained results with experimental data. This will be demonstrated in the Results section.

Modeling the active-passive transition

The primary difference in the corrosion behavior between carbon steels and 13%Cr steels is due to the formation of a protective passive film. Under favorable conditions, the 13%Cr steels remain passive and the corrosion rate remains low. However, passivity is affected by the presence of aggressive species in the solution such as chloride ions. Therefore, it is important to incorporate the active-passive transition in the model and, in particular, to relate the active-passive transition to the solution chemistry. For example, it is necessary to develop a relationship between the passive current density and the activities of aggressive species in the solution. In this way, the model will be capable of simulating rates of corrosion in either the passive or active state.

In a previous study,¹⁷ a simple model for the active-passive transition was proposed and applied to carbon steels in brine solutions with or without inhibitors. In this study, we extend this model to 13%Cr steels.

As originally proposed by Ebersbach et al.,²¹ the active-passive transition can be modeled by considering the current that leads to the formation of a passive layer in addition to the current that leads to active dissolution. At any instant, a certain fraction of the surface θ_p is assumed to be covered by the passive layer. The change of the passive layer coverage fraction with time can be expressed as

$$\left(\frac{\partial \theta_p}{\partial t} \right)_{E, a_i} = c i_2 (1 - \theta_p) - K \theta_p \quad (1)$$

where i_2 is the current density that contributes to the formation of a passive layer. The second term on the right-hand side of eq. (1) represents the rate of dissolution of the passive layer, which is proportional to the coverage fraction. The parameters c and K are proportionality constants. The total current density is expressed as

$$i_{Fe, TOT} = (i'_{Fe} + i_2)(1 - \theta_p) \quad (2)$$

where i'_{Fe} is the current density for active dissolution of iron. The total anodic current may be obtained by solving eqs. (1-2). In the stationary state ($t \rightarrow \infty$), the result is

$$i_{Fe, TOT} = \frac{i'_{Fe} + i_2}{1 + \frac{c i_2}{K}} = \frac{i'_{Fe} + i_2}{1 + \frac{i_2}{i_p}} \quad (3)$$

In eq. (3), the ratio c/K is equivalent to the passive current density. The current density i_2 can be represented by the usual expression for processes under activation control, i.e.,

$$i_2 = i_2^0 \exp\left(\frac{\alpha_2 F (E - E_F)}{RT}\right) \quad (4)$$

Thus, the model of the active-passive transition is characterized by three parameters, i.e., i_p , i_2^0 and α_2 . The i_p parameter is equal to the observable passive current density and the remaining two parameters are determined based on characteristics of the active-passive transition, i.e., the Flade potential and the critical current density.

The above formalism is useful for practical calculations once the parameters are coupled with solution chemistry. For example, chloride and other active ions cause the breakdown of passive films, which manifests itself in an increase in the passive current in addition to a possible onset of localized corrosion. On the other hand, some other ions may reinforce the passive behavior. In this study, we are not concerned with localized corrosion and examine only the effect of solution species on the dissolution rate in the passive state.

In the absence of active ions, the passive current density of many metals depends primarily on the pH of the solution.²² As shown by Vetter,²² the pH dependence of the corrosion current density in

the passive state is determined by a reaction between O^{2-} ions in the passive oxide layer and protons from the solution. In acidic solution, this dissolution reaction can be written as



where the symbol “ \equiv ” denotes the solid substrate and the formula $\equiv MeO_a(OH)_b$ represents the stoichiometry of a hydrated metal oxide in the passive layer. In general, the hydrated oxide is subject to compositional variations and the stoichiometry of reaction (5) may vary. Reaction (5) leads to a linear dependence of the passive current density on pH. For neutral and alkaline solutions, reaction (5) can be modified as



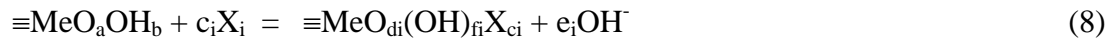
It should be noted here that reactions (5) and (6) could be, in principle, written for each constituent metal oxide in the alloy (e.g., for Fe and Cr). Then, the subsequent derivations could be made for individual alloy components. Such treatment, although detailed, would not be practical here because the dearth of quantitative experimental studies of the dissolution of 13%Cr steels precludes the evaluation of meaningful parameters. Therefore, it is more practical to treat $\equiv MeO_a(OH)_b$ in eqs. (5) and (6) as a general formula of a mixed oxide and neglect compositional variations as the oxide dissolves. With this assumption, our objective is to relate the rate of dissolution of the mixed oxide to the activities of solution species so that the dependence of the passive current density on solution chemistry can be reproduced in a semi-empirical manner. This assumption prevents us from considering the dissolution of individual alloy components. However, it allows us to develop a phenomenological treatment of the overall, averaged, dissolution process.

With the assumption discussed above, reactions (5) and (6) lead to an expression for the passive current density as a function of proton and water activities, i.e.,

$$i_p = k_H a_{H^+}^s + k_{H_2O} a_{H_2O}^u \quad (7)$$

Eq. (7) predicts a linear pH dependence of i_p in acidic solutions and a pH-independent value for nearly neutral solutions. As discussed in previous papers, this behavior is in good agreement with experimental results for the dissolution of iron.²²⁻²⁴ Analysis of polarization curves from various sources²⁵⁻³⁰ indicates that this result is also reasonable for 13%Cr steels.

To analyze the effect of active ions on the passive current density, we consider surface reactions between the passive oxide layer and the i -th ion from the solution, i.e.,



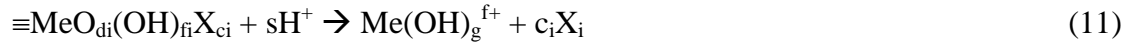
In eq. (8), the stoichiometry is usually difficult to define because of the dynamic nature of the system and may be, in general, fractional. In analogy with the theories of the dissolution of oxides in the bulk phase,³¹ it is reasonable to assume that eq. (8) is in quasi-equilibrium. Therefore, it may be characterized by an equilibrium constant, i.e.,

$$K_i = \frac{N_i a_{OH^-}^{e_i}}{(N_0 - \sum_k N_k) a_{X_i}^{c_i}} \quad i = 1, \dots, n \quad (9)$$

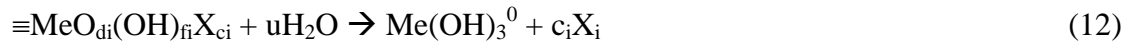
where the subscript i pertains to the i -th active ion, N_i is the number of sites per surface unit that are occupied by complexes containing the i -th active ion and N_0 is the total number of sites per surface area. Eq. (9) describes a system of equations that represent surface reactions involving any number of active species. This system may be solved with respect to N_i , i.e.,

$$N_i = \frac{N_0 K_i \frac{a_{X_i}^{c_i}}{a_{OH^-}^{e_i}}}{1 + \sum_k K_k \frac{a_{X_k}^{c_k}}{a_{OH^-}^{e_k}}} \quad (10)$$

The surface reaction (8) is followed by a dissolution reaction. Accordingly, the surface species that forms as a result of reaction (8) may undergo dissolution reactions that are analogous to reactions (5) or (6), i.e.,



and



On the right-hand side of eqs. (11) or (12), the active anions may further form aqueous complexes with the hydrolyzed iron cations.

In acidic solutions, the dissolution rate for the sites occupied by complexes with active ions is given, according to eq. (11), by

$$i_{p,i} = k_i N_i a_{H^+}^s \quad (13)$$

whereas the dissolution rate for the free sites is

$$i_{p,0} = k'_H \left(N_0 - \sum_k N_k \right) a_{H^+}^s \quad (14)$$

The total current density in the passive state is given by the sum of eqs. (13) and (14), i.e.,

$$i_p = i_{p,0} + \sum_k i_{p,k} \quad (15)$$

Analogous expressions can be written for the active species-assisted dissolution in neutral and alkaline solutions (eq. 12). Assuming that the surface reactions (eq. 8) are characterized by the same parameters over the whole pH range, the total passive current density can be expressed as

$$i_p = \left(k_H a_{H^+}^s + k_{H_2O} a_{H_2O}^u \right) \frac{1 + \sum_i l_i \frac{a_{X_i}^{c_i}}{a_{OH^-}^{e_i}}}{1 + \sum_i K_i \frac{a_{X_i}^{c_i}}{a_{OH^-}^{e_i}}} \quad (16)$$

where l_i is a composite parameter that contains both the forward dissolution rate constant (k_i) and the quasi-equilibrium constant K_i . In eq. (16), the k_H and k_{H_2O} parameters are determined using data for passive film dissolution in the absence of active ions. Then, the parameters l_i and K_i are determined by considering the effect of active species (e.g., chloride ions) on the passive current density.

The passive current density depends on temperature. Therefore, the parameters k_H and k_{H_2O} are assumed to be temperature-dependent by introducing a non-zero enthalpy of activation, i.e.,

$$k_H = k_H(T_{ref}) \exp \left[-\frac{\Delta H}{R} \left(\frac{1}{T} - \frac{1}{T_{ref}} \right) \right] \quad (17)$$

$$k_{H_2O} = k_{H_2O}(T_{ref}) \exp \left[-\frac{\Delta H}{R} \left(\frac{1}{T} - \frac{1}{T_{ref}} \right) \right] \quad (18)$$

where, for simplicity, the same enthalpy of activation is used for both parameters. The parameters l_i and K_i can be assumed to be temperature-independent.

Implementation of the model

To compute corrosion rates using the above model, the individual processes are combined and the corrosion potential is calculated by applying the mixed-potential theory. For this purpose, the conservation-of-charge equation is solved, i.e.,

$$\sum i_{c,i} = \sum i_{a,j} \quad (18)$$

where $i_{c,i}$ and $i_{a,j}$ denote the i -th cathodic and j -th anodic process. Eq. (18) is solved to obtain the corrosion potential, which is then used to calculate the corrosion rate. Additionally, the program incorporates a facility to plot the current density versus potential relationships for each individual anodic and cathodic process and for the overall process. Such plots facilitate the analysis of the relative importance of the partial processes.

Application of the model requires the regression of parameters that determine the numerical values of the current densities for all partial processes as a function of the potential. These parameters include the exchange current densities, energies of activation and reaction orders for partial anodic and cathodic processes and parameters of eqs. (4) and (16), which define the active-passive transition and

the dissolution in the passive state as a function of solution chemistry. The determination of these parameters for carbon steels was described in previous papers.^{15,16} For 13%Cr steels, the parameters have been determined by utilizing corrosion rate and polarization curve data in selected systems. Data for aqueous acids, bases and salt solutions³²⁻³⁴ were used to determine the parameters of the model in the absence of CO₂ and H₂S. Then, data for CO₂ systems^{25-27, 35-42} were used to evaluate the parameters of partial processes that are specific to CO₂ corrosion (i.e. the exchange current density and activation energy for carbonic acid reduction). Finally, parameters for partial processes that are influenced by H₂S were evaluated using data for mixed H₂S/CO₂ systems.^{36,40, 43-44}

RESULTS AND DISCUSSION

The model has been applied to simulate the rates of general corrosion of carbon steel and 13%Cr stainless steels in CO₂-containing aqueous systems, which may include various concentrations of chlorides, hydrogen sulfide and acetic acid. The results for carbon steel were extensively discussed in previous papers.^{15,16} In this study, we focus on the corrosion rates of 13%Cr steels. When appropriate, we compare the calculated corrosion rates for 13%Cr steels with those for carbon steels.

Figure 1 shows the effect of temperature on the corrosion rate of carbon steel (upper diagram) and 13%Cr steel (lower diagram) in moderately saline systems with a partial pressure of CO₂ equal to 30 bar. In the case of carbon steel, the observed maximum is a result of the temperature dependence of the protectiveness of the FeCO₃ surface layer. At low and moderate temperatures, the model predicts a low effective FeCO₃ coverage fraction. Then, the corrosion rate increases because the rates of the partial cathodic and anodic processes increase with temperature. However, the coverage fraction rapidly increases with temperature with most of the change occurring between approximately 50 and 120 °C. As discussed in a previous study,¹⁶ the protectiveness of the FeCO₃ layer can be related to the temperature dependence of the solubility of FeCO₃. Therefore, the corrosion rate reaches a maximum and then declines. In the case of the 13%Cr steel, the temperature dependence of the corrosion rate follows a completely different pattern in which a maximum is not observed. Instead, the rate generally increases with temperature although it somewhat levels off above 200 °C. This indicates that the protectiveness of FeCO₃ is not the determining factor for 13%Cr steels. The increase in the corrosion rate is primarily due to the increase in the passive current density with temperature (eqs. 17-18). Although experimental data from various data sets show some scattering, they are in agreement with the model results.

Since the corrosion rate of the 13%Cr steel is determined by the protectiveness of the passive film, the concentration of chloride ions has a significant effect on the rate. This is shown in Figure 2 for solutions with varying NaCl concentrations, in which the partial pressure of CO₂ is maintained at 30 bar and the temperature is 150 °C. In this case, a significant increase in the rate is observed as a function of chloride concentration. The increase is in agreement with experimental data.

It is worthwhile to examine the predicted current density versus potential relationships, which illustrate how the model reproduces the Cl⁻ ion effect. For this purpose, two sample *i-E* diagrams are shown in Figure 3. As shown in the figure, the anodic process of metal dissolution (denoted by the dotted line marked with “4”) shows an active-passive transition. The diagrams include three cathodic processes, i.e., the reduction of protons (marked by “1”), reduction of water (marked by “2”) and reduction of carbonic acid (marked by “3”). In view of the high partial pressure of CO₂, the reduction of carbonic acid is by far the dominant cathodic process. In a Cl⁻-free solution (upper diagram in

Figure 3), the metal is predicted to be in the passive state. In a 4.3 m NaCl solution (lower diagram), the passive current density is markedly increased and the metal dissolves in the active state. The change in the passive current density is modeled in accordance with eq. (16). It should be noted that the current version of the model is limited to general corrosion and, therefore, does not include the breakdown potential. Therefore, the passivity range in the lower diagram of Figure 3 extends to higher potentials than it would in reality.⁴² However, this limitation does not affect the computation of the rates of general corrosion.

Figures 4 and 5 show the dependence of the corrosion rate on the partial pressure of CO₂ for carbon steel and 13%Cr steel, respectively. In the case of carbon steel, the logarithm of the corrosion rate is proportional to the logarithm of CO₂ partial pressure at low and moderate temperatures. This regularity has been well established in the literature¹ and is reproduced by the model. In view of the model, this dependence is due to the cathodic process of carbonic acid reduction. The rate of carbonic acid reduction is proportional to the concentration of carbonic acid, which is roughly proportional to the partial pressure of CO₂. In the case of 13%Cr steel in solutions with high concentrations of chloride ions, a somewhat similar proportionality is also observed, although the slope of the log(rate)-log(P_{CO₂}) relationship is smaller. This is shown in Figure 5 for a 5.05 m chloride solution. The dependence of the corrosion rate on the CO₂ partial pressure is consistent with the predicted current density vs. potential relationship in the lower diagram of Figure 3. For highly saline solutions, the model predicts that the metal corrodes in the active state. Then, the corrosion rate depends on the rate of the reduction of carbonic acid (denoted by the dotted line marked with “3” in Figure 3). Since the rate of carbonic acid reduction is proportional to the partial pressure of CO₂, the corrosion rate should depend on P_{CO₂} as shown in Figure 5. On the other hand, corrosion in the passive state is predicted for systems with low concentrations of chloride ions (cf. the upper diagram in Figure 3). In this case, the corrosion rate is predicted to be only weakly dependent on the CO₂ partial pressure because the reaction of carbonic acid reduction is no longer a controlling process. This is consistent with experimental data, which are fairly scattered in chloride-free solutions and do not show an increase with the CO₂ partial pressure.³⁹

It is of particular interest to examine the performance of the model for systems containing both CO₂ and H₂S. Results of calculations for both iron and 13%Cr steel in a 0.9m NaCl solution in the presence of 30 bar CO₂ and varying amounts of H₂S are shown in Figure 6. As discussed in previous papers,¹⁵⁻¹⁶ the effect of hydrogen sulfide on carbon steels can be modeled by considering (1) the formation of FeS scales, (2) an additional cathodic process of H₂S reduction and (3) an additional contribution to the anodic dissolution of iron, which is mediated by the adsorption of HS⁻ ions. These three effects account for the dependence of the corrosion rate of iron on temperature and partial pressure of H₂S, which is shown in the upper diagram of Figure 6. Without H₂S, the corrosion rate shows a maximum that is characteristic of the effect of FeCO₃ scaling. With a low concentration of H₂S (i.e., 3.3 ppm), the maximum remains, but the peak becomes somewhat wider. With a higher concentration of H₂S (i.e., 330 ppm), the maximum essentially disappears and the corrosion rate becomes weakly dependent on temperature. At intermediate temperatures, the rate is substantially lower than in the presence of only CO₂. This is due to the fact that FeS becomes the predominant species on the surface of the metal and the temperature dependence of the FeS scale formation is much weaker than that of FeCO₃ formation. The disappearance of the maximum is consistent with experimental data,³⁶ although the predicted rates are somewhat lower than the data in the low temperature range. However, this difference is acceptable in view of the differences between various sets of experimental data.^{36,45}

In the case of the 13%Cr steel, the effect of H₂S is qualitatively different as shown in the lower diagram of Figure 6. The presence of H₂S consistently increases the corrosion rate at lower and moderate temperatures and the effect of H₂S diminishes as the temperature increases. There is no reduction in the corrosion rate that could be related to the formation of FeS layers. This is analogous to the lack of the effect of FeCO₃ scale formation on the corrosion rate in CO₂-only systems (cf. Figure 1). On the other hand, the substantial increase in the rate at low and moderate temperatures is due to a combination of the cathodic process of H₂S reduction and the additional contribution to anodic dissolution, which is mediated by the adsorption of HS⁻ ions. As shown in Figure 6, the model reproduces the observed corrosion rate pattern with good accuracy.

Finally, the model has been applied to systems that contain acetic acid in addition to carbon dioxide. Acetic acid contributes to the cathodic process since it can act as a donor of protons. At the same time, it can enter into surface reactions with the passive film (cf. eq. 16), which can increase the passive current density. Figure 7 shows the predicted concentration dependence of the corrosion rate of 13%Cr steel in boiling acetic acid solutions. Figure 8 shows the effect of 0.5 wt.% of acetic acid on the corrosion rate in a 0.9m NaCl solution with a CO₂ partial pressure of 30 bar. As shown in the figure, even a small amount of acetic acid appreciably increases the corrosion rate of 13%Cr steel. The results of model calculations agree with experimental data within the limit of data scattering.

CONCLUSIONS

A comprehensive model has been developed for simulating the effect of environmental variables on the rates of general corrosion of carbon steel and 13%Cr stainless steel. The model combines thermodynamic speciation calculations with electrochemical computations based on the mixed-potential theory. The electrochemical calculations recognize the effects of various partial cathodic and anodic processes and incorporate a model for active-passive transition. The model has been verified by comparing calculated corrosion rates with experimental data over substantial ranges of temperature, pressure and solution composition. In particular, the effects of salinity, hydrogen sulfide and acetic acid on CO₂ corrosion can be simulated. Very good agreement with experimental data has been obtained. Thus, the model can be used as a predictive tool for multicomponent systems for which experimental data are not available.

REFERENCES

1. C. de Waard, D. E. Milliams, *Corrosion*, v. 31, p. 177-181 (1975).
2. C. de Waard, U. Lotz, D. E. Milliams, *Corrosion*, v. 47, p. 976 (1991).
3. S. Kanwar, W. P. Jepson, *CORROSION/94*, paper no. 24, NACE International, Houston, TX (1994).
4. R. Zhang, M. Gopal, W. P. Jepson, *CORROSION/97*, paper no. 601, NACE International, Houston, TX (1997).
5. L. K. Gatzky, R. H. Hausler, "A Novel Correlation of Tubing Corrosion Rates and Gas Production Rates", in R.H. Hausler, H. P. Godard, *Advances in CO₂ Corrosion*, Vol. 1, p. 87, NACE International, Houston, TX (1984).
6. J.-L. Crolet, M. R. Bonis, "A Tentative Method for Predicting the Corrosivity of Wells in New CO₂ Fields", in P. A. Burke, A. I. Asphahani, B. S. Wright, *Advances in CO₂ Corrosion*, Vol. 2, p. 23, NACE International, Houston, TX (1985).

7. M. R. Bonis, J.-L. Crolet, CORROSION/89, paper no. 466, NACE International, Houston, TX (1989).
8. R. H. Hausler, J. D. Garber, CORROSION/90, paper no. 45, NACE International, Houston, TX (1990).
9. J. D. Garber, F. H. Walters, R. R. Alapati, C. D. Adams, CORROSION/94, paper no. 25, NACE International, Houston, TX (1994).
10. S. Nesic, J. Postlethwaite, S. Olsen, Corrosion, v. 52, p. 280-294 (1996).
11. S. Srinivasan, R. D. Kane, CORROSION/96, paper no. 11, NACE International, Houston, TX (1996).
12. A. Dugstad, L. Lunde, K. Videm, CORROSION/94, paper no. 14, NACE International, Houston, TX (1994).
13. R. C. John, K. G. Jordan, A. L. Young, S. D. Kapusta, W. T. Thompson, CORROSION/98, paper no. 20, NACE International, Houston, TX (1998).
14. E. Dayalan, F. D. de Moraes, J. R. Shadley, S. A. Shirazi, E. F. Rybicki, CORROSION/98, paper no. 51, NACE International, Houston, TX (1998).
15. A. Anderko and R. D. Young, CORROSION/99, paper no. 31, NACE International, Houston, TX (1999).
16. A. Anderko, CORROSION/2000, paper no. 102, NACE International, Houston, TX (2000).
17. A. Anderko and R. D. Young, Corrosion, v. 56, p. 543-555 (2000).
18. A. Anderko, P. McKenzie and R. D. Young, Corrosion, in press (2001).
19. J.F. Zemaitis, Jr., D. M. Clark, M. Rafal, N. C. Scrivner, Handbook of aqueous electrolyte thermodynamics: AIChE, New York, NY, 852 p. (1986).
20. M. Rafal, J. W. Berthold, N. C. Scrivner, S. L. Grise, Models for electrolyte solutions, *in* S. I. Sandler, ed., Models for Thermodynamic and Phase Equilibria Calculations: M. Dekker, New York, NY, p. 601-670 (1995).
21. U. Ebersbach, K. Schwabe, K. Ritter, Electrochim. Acta, v. 12, p. 927-938 (1967).
22. K. J. Vetter, Electrochemical Kinetics: Academic Press, New York, NY (1967).
23. N. Sato, T. Noda, K. Kudo, Electrochim. Acta, v. 19, p. 471-475 (1974).
24. K. J. Vetter, Z. Elektrochem., v. 59, p. 67 (1955).
25. A. Ikeda, M. Ueda, S. Mukai, *in* R. H. Hausler and H. P. Godard, eds., Advances in CO₂ Corrosion, Vol. 1: NACE, Houston, TX, p. 39-51 (1984).
26. M. Matsui, A. Kuhara, A. Yoshitake, T. Ishii, *in* R. H. Hausler and H. P. Godard, eds., Advances in CO₂ Corrosion, Vol. 1: NACE, Houston, TX, p. 130-142 (1984).
27. B. R. Linter, G. T. Burstein, Corros. Sci., v. 41, p. 117 (1999).
28. S. Huizinga, W. E. Like, Corrosion, v. 50, p. 555 (1994).
29. T. Motooka, Y. Sugie, S. Fujii, Corrosion, v. 48, p. 540 (1992).
30. M. A. A. Tullmin, F. P. A. Robinson, Corrosion, v. 44, p. 664 (1988).
31. M. A. Blesa, P. J. Morando, A. E. Regazzoni, Chemical Dissolution of Metal Oxides: CRC Press, Boca Raton, FL (1994).
32. D. Behrens, ed., DECHEMA Corrosion Handbook, Vols. 1-12: VCH Verlagsgesellschaft, Weinheim, Germany (1987-1992)
33. B. D. Craig, D. S. Anderson, eds., Handbook of Corrosion Data: ASM International, Materials Park, OH (1995).
34. L. L. Shreir, ed., Corrosion, Metal/Environment Reactions, Vol. 1, Newness-Butterworth, Boston (1976).
35. K. Masamura, S. Hashizume, K. Nunomura, J.-I. Sakai and I. Matsushima, *in* R. H. Hausler and H. P. Godard, eds., Advances in CO₂ Corrosion, Vol. 1: NACE, Houston, TX, p. 143-150. (1984).

36. A. Ikeda, M. Ueda, S. Mukai, *in* P. A. Burke, A. I. Asphahani and B. S. Wright, eds., *Advances in CO₂ Corrosion*, Vol. 2: NACE, Houston, TX, p. 1-22 (1985).
37. M. Ueda and H. Takabe, *CORROSION/98*, paper no. 35: NACE International, Houston, TX (1998).
38. A. Ikeda, S. Mukai and M. Ueda, *in* P. A. Burke, A. I. Asphahani and B. S. Wright, eds., *Advances in CO₂ Corrosion*, Vol. 2: NACE, Houston, TX, p. 47-54 (1985).
39. J. B. Bryant and G.B. Chitwood, *in* R. H. Hausler and H. P. Godard, eds., *Advances in CO₂ Corrosion*, Vol. 1: NACE, Houston, TX, p. 163-172 (1984).
40. B. Lefebvre, G. Guntz, J. C. Prouheze, J. C. Vaillant, J. R. Mantelle, P. Bounie and J P. Giraud, *in* L.E. Newton and R. H. Hausler, eds., *CO₂ Corrosion in Oil and Gas Production*, NACE, Houston, TX, p. 295-307 (1984).
41. B. Lefebvre, G. Guntz, J. C. Prouheze, J. J. Renault and P. Bounie, *in* P. A. Burke, A. I. Asphahani and B. S. Wright, eds., *Advances in CO₂ Corrosion*, Vol. 2: NACE, Houston, TX, p. 55-71 (1985).
42. K. Masamura, S. Hashizume, J. Sakai, I. Matsushima, *Corrosion*, v. 43, p. 359 (1987).
43. G. Fierro, G. M. Ingo, F. Mancina, *Corrosion*, v. 45, p. 814 (1989).
44. H. Kurahashi, T. Kurisu, Y. Sone, K Wada, Y. Nakai, *Corrosion*, v. 41, p. 211 (1985).
45. E. C. Greco, W. B. Wright, *Corrosion*, v. 18, p. 119t-124t (1962).

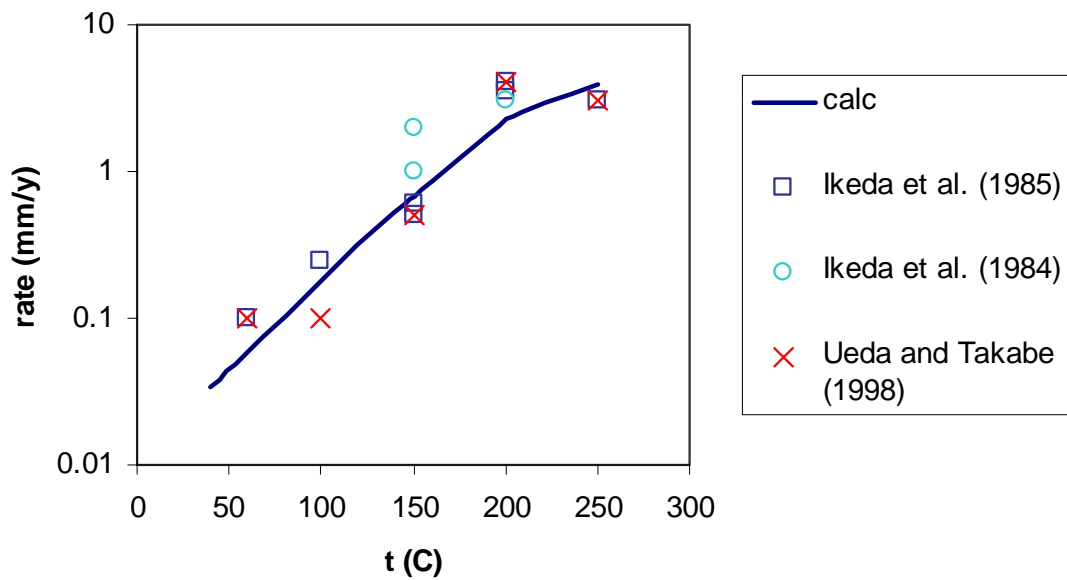
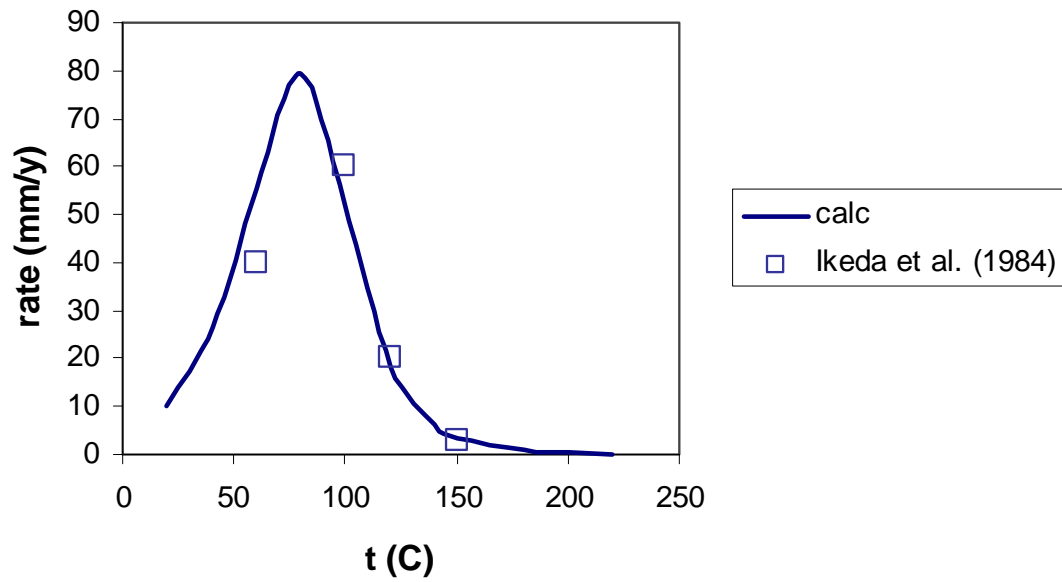


Figure 1. Effect of temperature on the corrosion rate of carbon steel (upper diagram) and 13% Cr stainless steel (lower diagram) in systems with a CO₂ partial pressure of 30 bar. The results in the upper and lower diagrams have been obtained for simulated seawater and 0.9 m NaCl solution, respectively. The symbols denote the experimental data of Ikeda et al.^{25, 38} and Ueda and Takabe.³⁷

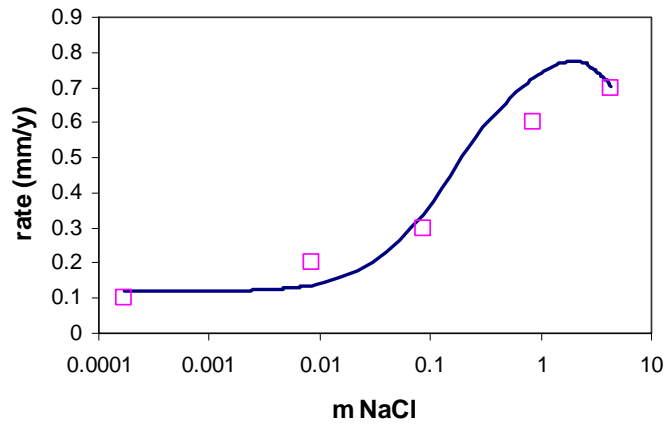


Figure 2. Effect of NaCl concentration on the corrosion rate of 13% Cr steel in a system with a CO₂ partial pressure equal to 30 bar at 150 °C. The symbols denote the experimental data of Ikeda et al.³⁸ and the line has been obtained from the model.

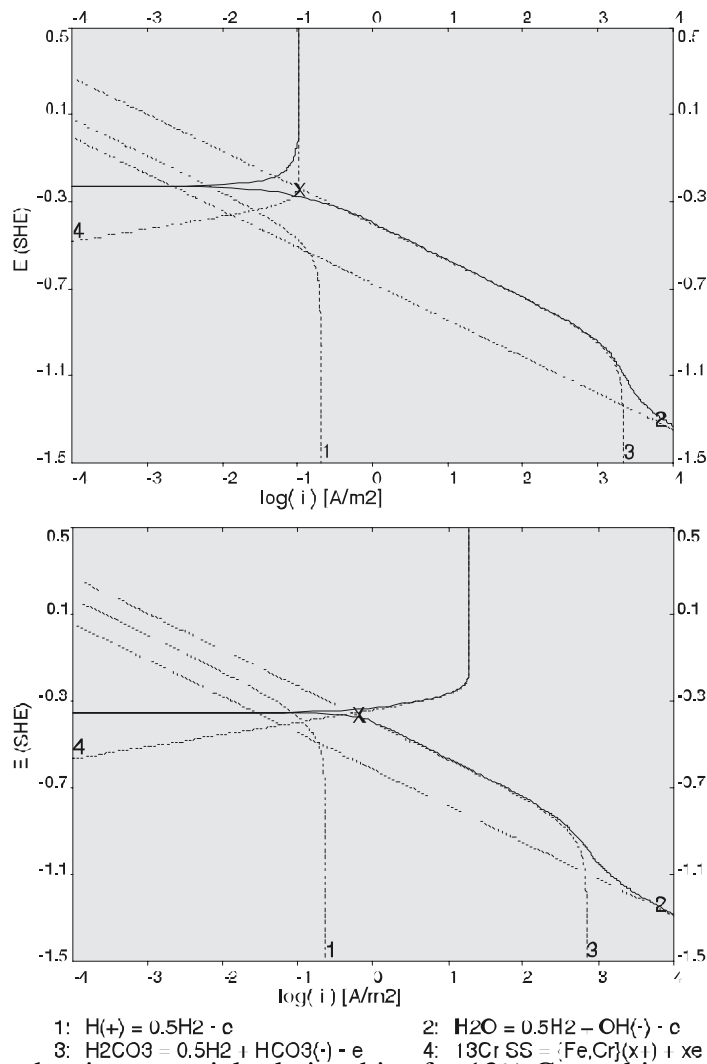


Figure 3. Predicted current density-potential relationships for 13% Cr steel in systems with a CO₂ partial pressure of 30 bar at 150 °C. The upper diagram has been generated for an NaCl-free solution and the lower diagram for a 4.3 m NaCl solution.



Figure 4. Effect of the partial pressure of CO₂ on the corrosion rate of carbon steel in a 0.1% NaCl solution at various temperatures. The symbols represent experimental data¹ and the lines have been obtained from the model.

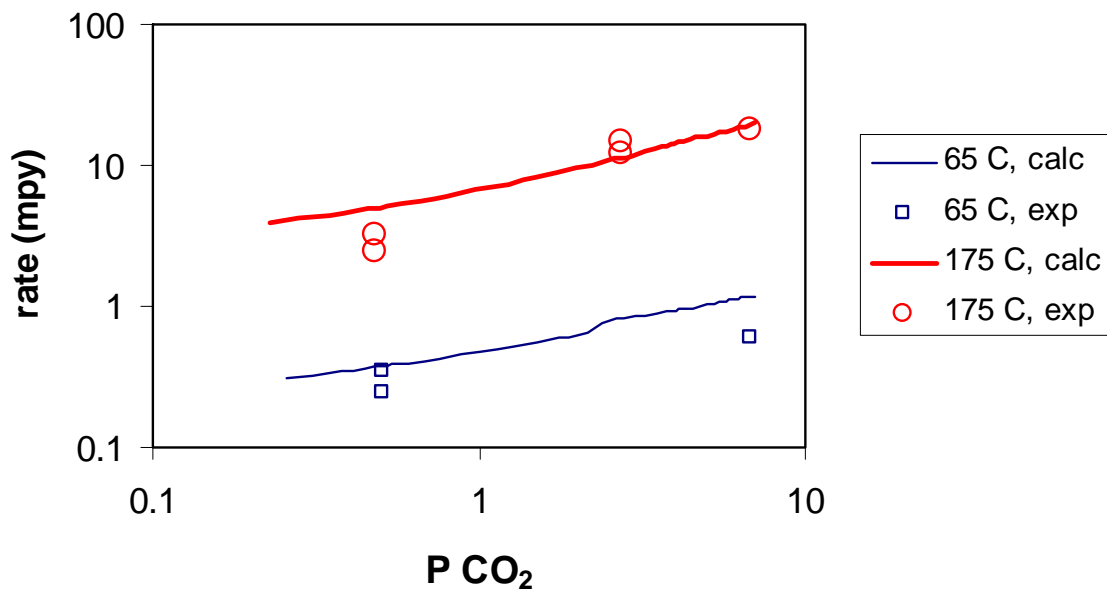


Figure 5. Effect of the partial pressure of CO₂ on the corrosion rate of 13% Cr steel in a 15.2% (5.05m) chloride solution at two temperatures. The symbols represent experimental data³⁹ and the lines have been obtained from the model.

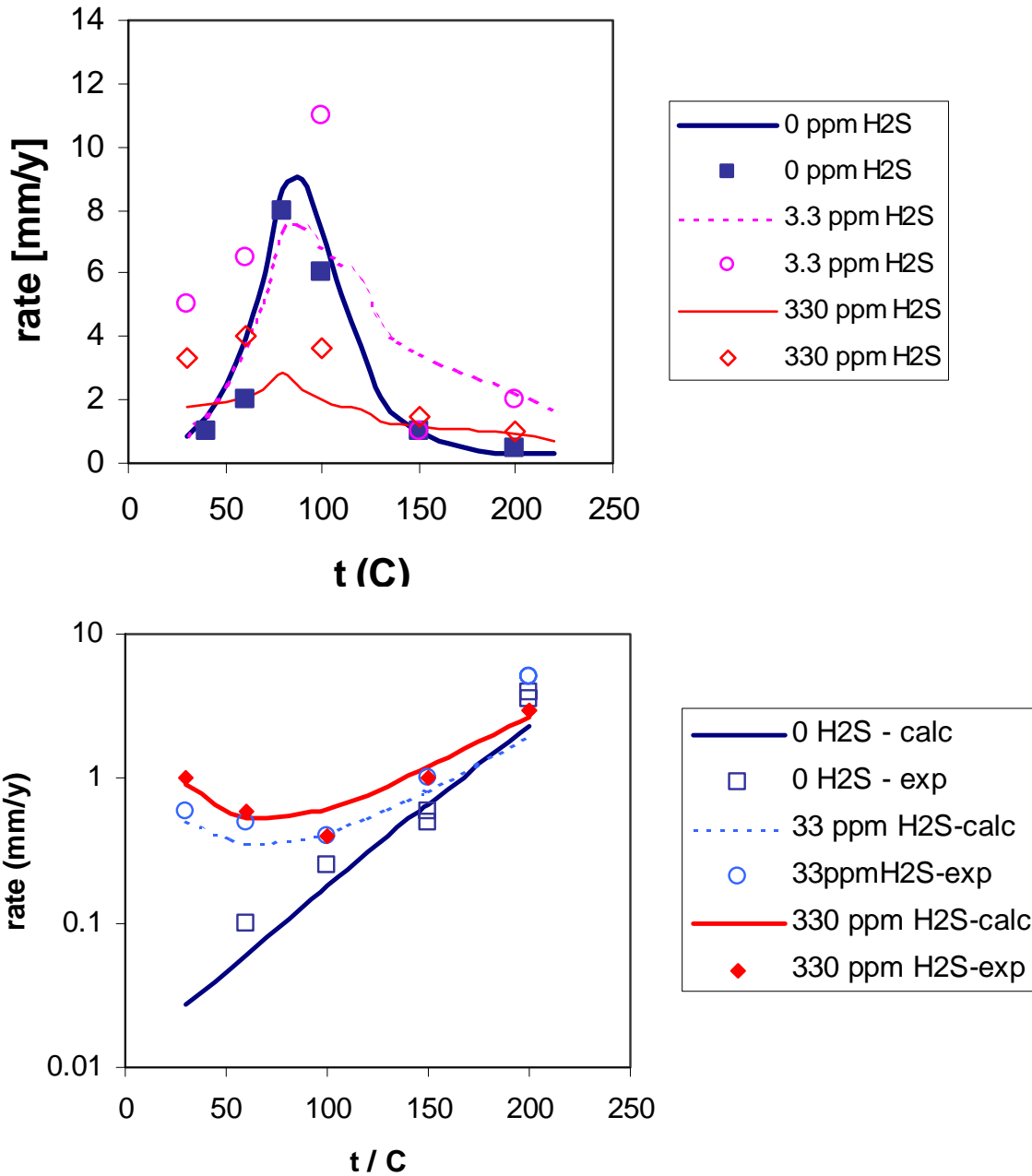


Figure 6. Effect of H₂S concentration on the corrosion rate of iron (upper diagram) and 13% Cr stainless steel (lower diagram) as a function of temperature in a 0.9 m NaCl solution with a partial pressure of CO₂ equal to 30 bar. The lines have been calculated using the model and the symbols denote the data of Ikeda et al.³⁶

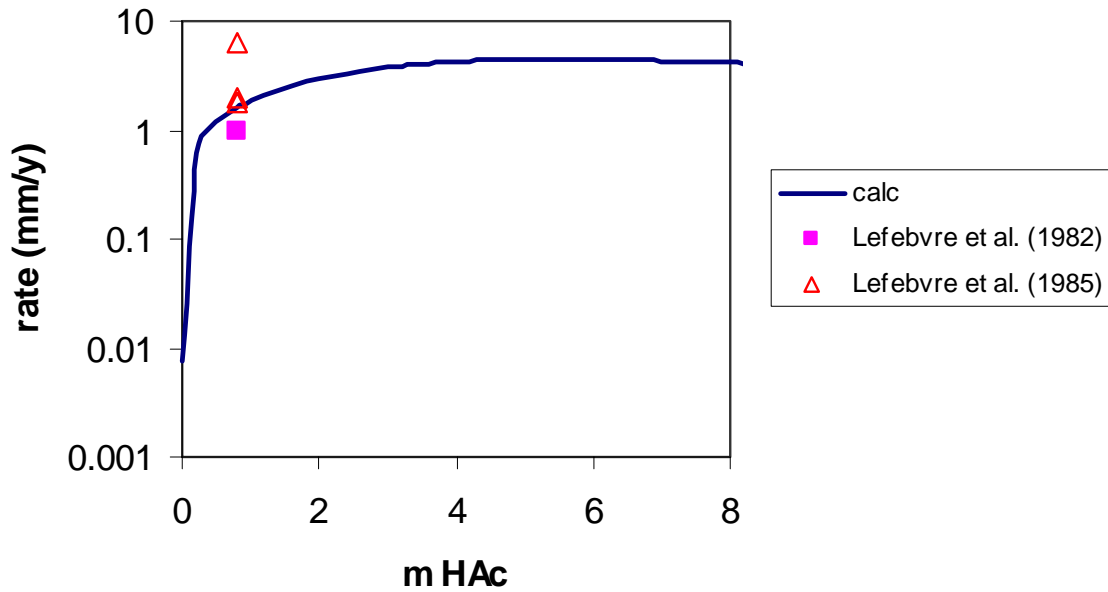


Figure 7. Corrosion rate of 13% Cr stainless steel in boiling acetic acid as a function of acid concentration. The symbols represent experimental data^{40,41} and the lines have been obtained from the model.

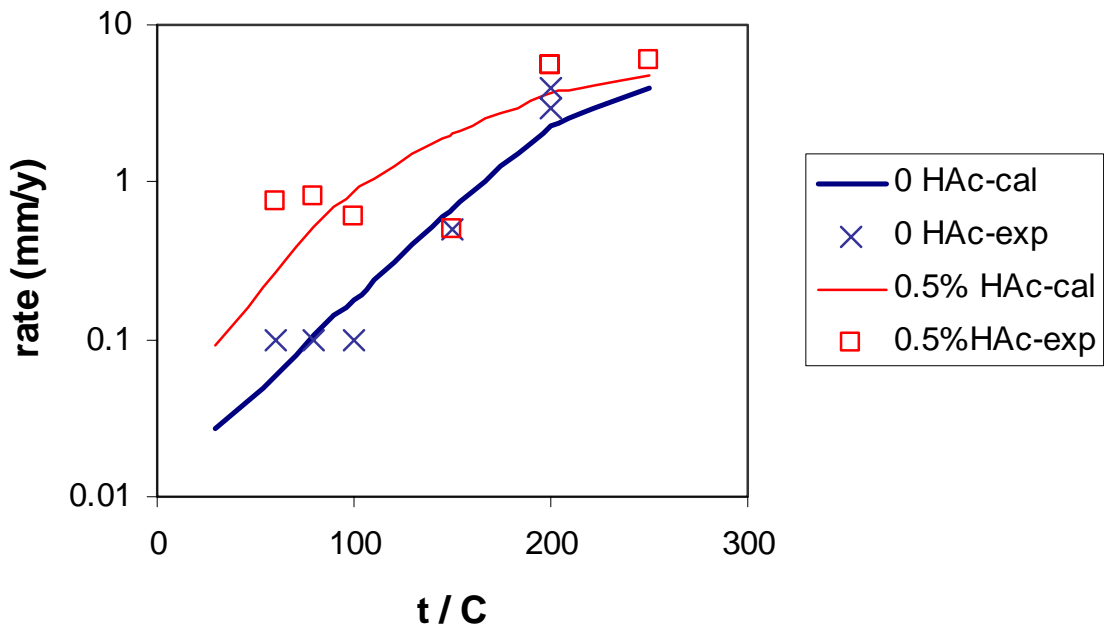


Figure 8. Effect of acetic acid on the corrosion rate of 13% Cr stainless steel as a function of temperature in a 0.9 m NaCl solution with a partial pressure of CO₂ equal to 30 bar. The symbols denote the experimental data of Ueda and Takabe³⁷ for systems without and with 0.5% (0.088 m) acetic acid and the lines represent the results of calculations.